22. Richardson, M. I., Wilson, R. J. & Rodin, A. V. Water ice clouds in the Martian atmosphere: General circulation model experiments with a simple cloud scheme. *J. Geophys. Res.* (submitted).

23. Ward, W. R. in *Mars* (eds Kieffer, H. H., Jakosky, B. M., Snyder, C. W. & Matthews, M. S.) 298–320 (Univ. Arizona Press, Tucson, 1992).

24. Herkenhoff, K. E. & Plaut, J. J. Surface ages and resurfacing rates of the polar layered deposits on Mars. *Icarus* **144**, 243–253 (2000).

25. Fenton, L. K. & Richardson, M. I. Martian surface winds: Insensitivity to orbital changes and implications for aeolian processes. *J. Geophys. Res.* **106**, 32885–32902 (2001).

26. Jakosky, B. M., Henderson, B. G. & Mellon, M. T. The Mars water cycle at other epochs—Recent history of the polar caps and layered terrain. *Icarus* **102**, 286–297 (1993).

....

Ferromagnetism in one-dimensional monatomic metal chains

P. Gambardella*, **A. Dallmeyer**†, **K. Maiti**†, **M. C. Malagoli**†, **W. Eberhardt**†‡, **K. Kern***§ **& C. Carbone**†‖

* *Institut de Physique des Nanostructures, EPF-Lausanne, CH-1015 Lausanne, Switzerland*
† *Institut für Festkörperforschung, Forschungszentrum Jülich, D-52425 Jülich, Germany*
‡ *Berliner Elektronenspeicherring-Gesellschaft für Synchrotronstrahlung m.b.H., Albert-Einstein-Straße 15, 12489 Berlin, Germany*
§ *Max-Planck-Institut für Festkörperforschung, Heisenbergstr. 1, D-70569 Stuttgart, Germany*
‖ *Istituto di Struttura della Materia, Consiglio Nazionale delle Richerche, Area Science Park, I-34012 Trieste, Italy*

....

Two-dimensional systems, such as ultrathin epitaxial films and superlattices, display magnetic properties distinct from bulk materials[1]. A challenging aim of current research in magnetism is to explore structures of still lower dimensionality[2–6]. As the dimensionality of a physical system is reduced, magnetic ordering tends to decrease as fluctuations become relatively more important[7]. Spin lattice models predict that an infinite one-dimensional linear chain with short-range magnetic interactions spontaneously breaks up into segments with different orientation of the magnetization, thereby prohibiting long-range ferromagnetic order at a finite temperature[7–9]. These models, however, do not take into account kinetic barriers to reaching equilibrium or interactions with the substrates that support the one-dimensional nanostructures. Here we demonstrate the existence of both short- and long-range ferromagnetic order for one-dimensional monatomic chains of Co constructed on a Pt substrate. We find evidence that the monatomic chains consist of thermally fluctuating segments of ferromagnetically coupled atoms which, below a threshold temperature, evolve into a ferromagnetic long-range-ordered state owing to the presence of anisotropy barriers. The Co chains are characterized by large localized orbital moments and correspondingly large magnetic anisotropy energies compared to two-dimensional films and bulk Co.

Since the work of Ising[8], magnetism in one-dimensional (1D) systems has been the subject of continuous theoretical[4,5,7–10] and experimental[2,6,11] research. Progress in atomic engineering makes it possible today to build 1D arrays of transition-metal chains by self-

assembly epitaxial techniques on suitable substrates[12,13]. Pioneering experiments[14–16] in this direction investigated the magnetic behaviour of Fe stripes 1–10 nm wide obtained by step-flow growth on W(110) and Cu(111) surfaces. Ideally, one would like to construct monatomic chains in very large numbers while maintaining a fine control on the dimensions, uniformity and spatial distribution of the individual chains. We have shown[17] that it is possible to produce high-density (5×10^6 cm^{-1}) arrays of parallel monatomic chains with unprecedented uniformity and even spacing by growing Co on a high-quality Pt vicinal surface in a narrow (250–300 K) temperature range. The scanning tunnelling microscopy (STM) images in Fig. 1 illustrate the regular step structure of the vicinal Pt(997) surface (Fig. 1a) and the fabrication of monatomic Co wires by decoration of the steps (Fig. 1b)[17].

The magnetism of the Co wires has been investigated by X-ray magnetic circular dichroism[18] (XMCD) at beamline ID-12B of the European Synchrotron Radiation Facility in Grenoble. Representative results for the circular dichroism in X-ray absorption spectroscopy (XAS) at the Co $L_{2,3}$ absorption edges for the monatomic wires are shown in Fig. 2a and compared with one monolayer (Fig. 2b) and bulk Co spectra (Fig. 2c). The difference between the two spectra for left- and right-handed polarization, reported in the lower panel, shows that the wires are characterized by a strong dichroism that results from the alignment of the Co magnetic moments in an external field of 7 T at 10 K. The amplitude of the dichroic signal is a measure of the magnetization of the Co wire array and contains information on the local character of the atomic moments.

The reduced atomic coordination of the monatomic chains compared to bulk Co and two-dimensional (2D) films has remarkable consequences for the relative size of the local orbital (m_L) and spin (m_S) magnetic moments. Both m_L and m_S are expected to increase as the atomic coordination is reduced in passing from the bulk to the monatomic chains. Local spin density calculations for Co/Pt(997) show that the narrowing of the Co 3d band and the
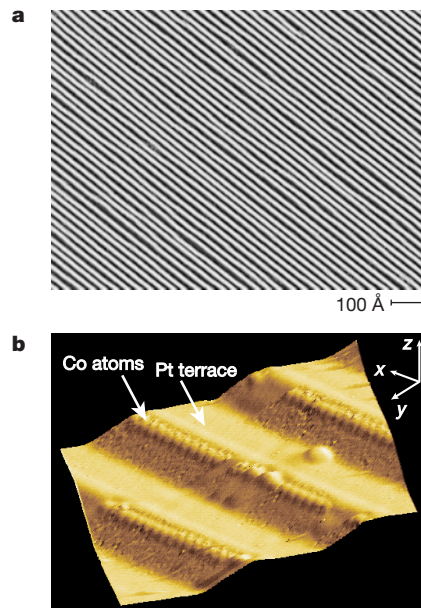
Figure 1 STM topographs of the Pt(997) surface. **a**, Periodic step structure (each white line represents a single step). The surface has a 6.45° miscut angle relative to the (111) direction; repulsive step interactions result in a narrow terrace width distribution centred at 20.2 Å with 2.9 Å standard deviation. **b**, Co monatomic chains decorating the Pt step edges (the vertical dimension is enhanced for better contrast). The monatomic chains are obtained by evaporating 0.13 monolayers of Co onto the substrate held at $T = 260$ K and previously cleaned by ion sputtering and annealing cycles in ultrahigh vacuum (UHV). The chains are linearly aligned and have a spacing equal to the terrace width.

301

corresponding increase in the density of states at the Fermi level produce the increase in m_S from the 1.57 μ_B per atom bulk value to 2.03 and 2.08 μ_B per atom for a monolayer and a 1D chain, respectively (G. Bihlmayer, X. Nie and S. Blügel, unpublished results); similar values can be found in refs 4 and 19). A larger relative increase is expected for m_L, which is generally more sensitive to changes in the atomic coordination because of its dependence on the crystal field. Using the XMCD sum rule[20], m_L can be determined from: $\int_{L_3+L_2}(\mu_+ - \mu_-)dE = (C/2\mu_B)m_L$, where μ_+ and μ_- are the absorption spectra for parallel and antiparallel direction of light polarization and magnetization, E is the photon energy and C is an experimental constant[18,21] that is determined from the known bulk value $m_L = 0.14\,\mu_B$ per atom[22] (Fig. 2c). For the monatomic wires we find $m_L = 0.68 \pm 0.05\,\mu_B$ per atom, an enhancement of about a factor of five compared to bulk Co. Dimensionality effects turn out to be decisive as we find that for biatomic wires and one monolayer Co m_L drops to 0.37 μ_B per atom and 0.31 $\pm$ 0.04 μ_B per atom, respectively. The m_L value determined for the monatomic chains represents the highest orbital moment found in a 3d itinerant electron system, and is considerably larger than that of typical 2D Co structures[23] and nanoscale Co clusters[24].

In Fig. 3a we report the magnetic response of a set of monatomic wires at $T = 45$ K. The zero remanent magnetization (M) at $B = 0$ reveals the absence of long-range ferromagnetic order. However, the shape of the magnetization curve indicates the presence of short-range order, and therefore of significant interatomic exchange coupling in the chains. For non-interacting paramagnetic moments the magnetization expected in the present experimental conditions would be significantly smaller, as indicated by the dotted line in Fig. 3a. The observed behaviour is that of a 1D superparamagnetic system, that is, a system composed by segments, or spin blocks, each containing N exchange-coupled Co atoms, whose magnetization
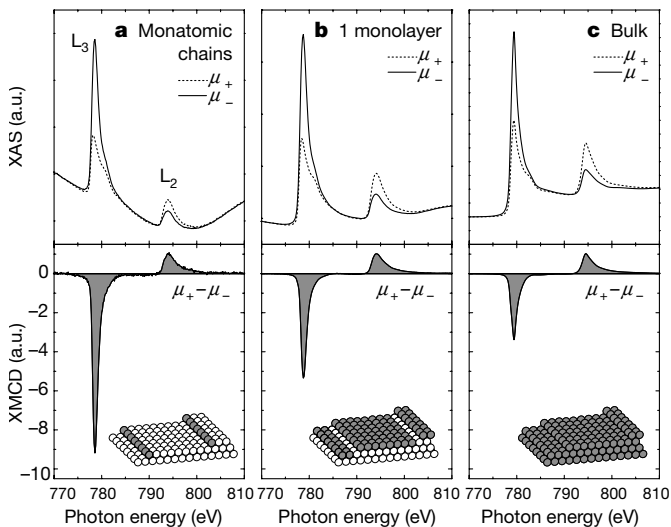
orientation is not stable owing to thermal fluctuations. A noticeable dependence of the magnetization on the direction of the applied field can be observed in Fig. 3. The strongest magnetic response is found in the direction pointing towards the step edges, perpendicular to the chain axis—at +43° from the (111) normal—as shown in the inset in Fig. 3a. Clearly, the shape of the superparamagnetic curves depends on the magnetic anisotropy energy of each spin block E_a, as well as on N times the magnetic moment per Co atom m, as in a paramagnetic system. According to classical Boltzmann statistics, the magnetization of an assembly of aligned particles with magnetic moment Nm and anisotropy E_a, placed in an external field B at an angle θ_0 with respect to the easy axis of magnetization is given by:

$$M = M_{sat}\frac{\int_0^{2\pi}d\varphi\int_0^\pi d\vartheta\,\sin\vartheta\,\cos\vartheta\,e^{(NmB\cos\vartheta+E_a(\sin\theta_0\sin\vartheta\cos\varphi+\cos\theta_0\cos\vartheta)^2)/kT}}{\int_0^{2\pi}d\varphi\int_0^\pi d\vartheta\,\sin\vartheta\,e^{(NmB\cos\vartheta+E_a(\sin\theta_0\sin\vartheta\cos\varphi+\cos\theta_0\cos\vartheta)^2)/kT}}$$

(1)

where ϑ and φ represent the spherical coordinates of Nm. By fitting the magnetization in Fig. 3a with equation (1), we obtain $Nm = 59 \pm 2\,\mu_B$ and $E_B = 31 \pm 1$ meV. To correctly determine the number of coupled Co atoms per chain, N, we have to divide the calculated Nm value by $m = m_{Co} + m_{Pt}$, where $m_{Co} = m_L + m_S = 2.8\,\mu_B$, and m_{Pt} represents the induced moment on the first- and second-nearest Pt neighbours. The latter amounts to about 1 μ_B per Co atom, as derived on the basis of experimental[25] and theoretical[19] results. Thus, we find that at 45 K about 15 Co atoms are coupled in each spin block, whereas the average length of a continuous Co chain (uninterrupted by kinks) is estimated to be about 80 atoms. The magnetic anisotropy energy (MAE) is 2.0 $\pm$ 0.2 meV per atom, a very large value compared to bulk h.c.p. Co (40 μeV per atom[26]) and compared to a Co monolayer on Pt(997) (0.14 $\pm$ 0.01 meV per atom). The MAE is directly related[21] to the anisotropy of m_L measured in the easy and hard directions, which is unusually large (0.12 μ_B) for the present system. The transition from 1D to a 2D system has profound effects on the magnetic anisotropy of the system: the MAE falls to 0.34 meV per atom for a bi-atomic chain and to 0.13 meV per atom for a Co monolayer film on Pt(997), a result that is related to the sharp decrease of the orbital magnetization reported above.

Here we cannot directly determine whether the measured size of the spin blocks is related to the occurrence of critical fluctuations in the 1D chains. We note, however, that the finite temperature and size of the chain system play a major role. A simple theoretical argument due to Landau[7] shows that finite 1D Ising chains with a number of ferromagnetically-coupled spins $N > \exp(2J/kT)$, with J
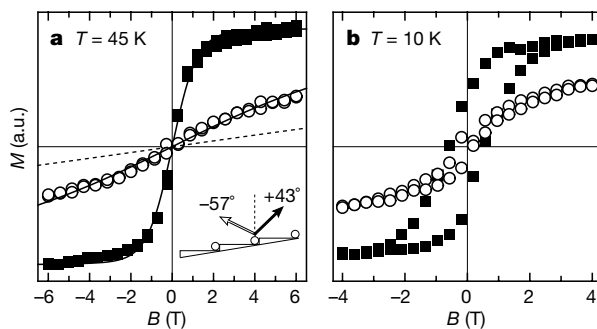

Figure 2 Co X-ray absorption spectra for parallel (μ_+) and antiparallel (μ_-) direction of light polarization and field-induced magnetization. The dichroism signal ($\mu_+ - \mu_-$) is obtained by subtraction of the absorption spectra in each panel and normalization to the L_2 peak. **a**, Monatomic chains; **b**, one monolayer; **c**, thick Co film on Pt(997). The sample was mounted onto a UHV variable-temperature insert that could be rotated with the respect to the direction of the external magnetic field applied parallel to the incident photon beam. Spectra were recorded in the electron-yield mode at $T = 10$ K and $B = 7$ T. Because of the low Co coverage, the edge structures of the monatomic wires are superimposed to a strong background originating from the oscillations following the Pt $N_{2,3}$ thresholds. As the structures from the non-magnetic substrate do not exhibit a dichroic effect, they do not contribute to the dichroic signal. Changes in the L_3 XMCD intensity indicate that the orbital moment is substantially increased in going from bulk Co to a 2D Co monolayer and, finally, to the 1D chains.

Figure 3 Magnetization of a monatomic wire array recorded at the L_3 Co edge. **a**, M as a function of the applied field at $T = 45$ K measured along the easy direction (filled squares) and at 80° away from the easy direction (open circles) in the plane perpendicular to the wire axis (see inset). The solid lines are fits to the data according to equation (1) with values $Nm = 59\,\mu_B$, $E_a = 31$ meV, $T = 45$ K. The dashed line represents the magnetization expected for an isolated Co atom with $N = 1$, $m = 4\mu_B$, $E_a = 2.1$ meV, $T = 45$ K. **b**, Hysteresis measured at $T = 10$ K below the blocking temperatures of the wires, in the same geometry as **a**.
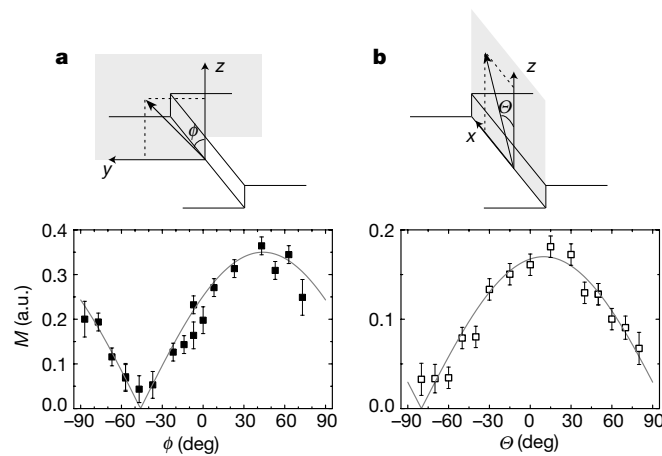
Figure 4 Angular dependence of the magnetization. **a**, Perpendicular; **b**, parallel to the wire axis at 10 K. For each angle the magnetization has been aligned in a 6 T magnetic field and subsequently measured near remanence at 0.25 T. A $|\cos(x - x_0)|$ dependence is found in both directions (solid lines), where $x = \Phi, \Theta$.

being the exchange energy between nearest-neighbour spins, break up spontaneously into smaller domains. Assuming the magnitude of $2J$ to be 15 meV (refs 6, 27), we get an upper limit of $N = 50$ atoms at $T = 45$ K. This argument, however, does not forbid the existence of ferromagnetism in finite 1D chains at finite temperature on the timescale of an experimental observation. As in bulk ferromagnetic systems, anisotropy energy barriers can effectively pin the magnetization along a fixed direction in space. Indeed, by lowering the sample temperature below 15 K, we observe a transition to a long-range ferromagnetically ordered state (Fig. 3b). Below the so-called blocking temperature ($T_B = 15 \pm 5$ K for the monatomic wires), the magnetization of each spin-block aligns in the easy axis direction, and the whole system becomes ferromagnetic. In a Néel–Brown model[28], the relaxation time of a single-domain magnetic particle is expressed by an Arrhenius law of the form $\tau = \tau_0 e^{-E_a/kT}$, where τ_0 is a prefactor of the order of 10^{-9} s. The determined anisotropy energy of $E_a = 31 \pm 1$ meV is thus consistent with the blocking temperature determined for the XMCD data, which yield a relaxation time $\tau \geq 10^2$ s at $T \leq 15$ K.

As in 2D films, the MAE and the easy axis of magnetization are determined by the wire atomic structure and by the substrate. Tight-binding MAE calculations of free-standing and Pd-deposited Co monatomic chains[5] show that the easy direction rotates from parallel to the chain axis to out-of-plane in passing from the free-standing to the Pd-supported chains. Here the 1D geometry of the wires and the interaction with the substrate are manifested by a strong uniaxial anisotropic behaviour. Figure 4 shows the magnetization measured near remanence ($B = 0.25$ T) along different directions of the incident light with respect to the sample normal. M follows a cosine function both in the plane perpendicular to the wire axis and in the plane parallel to the wires, with a maximum in the perpendicular plane at $+43°$. In our experiments we do not find evidence for interchain coupling effects[11] between the wires, either induced by the substrate or of dipolar origin. Ferromagnetic coupling between adjacent wires mediated by the polarization of the non-magnetic Pt host would result in an increase of the blocking temperature with respect to the value calculated by the Arrhenius law—such an increase is not observed. Interactions of dipolar origin, on the other hand, are far too weak (~0.06 meV between adjacent chains with perpendicular magnetization) compared to the MAE and also to thermal fluctuations ($kT \approx 4$ meV at 45 K and 0.8 meV at 10 K).

One-dimensional models are known to be useful in analysing many-body problems, but it is only recently that 1D systems made of real atoms have become the object of experiments. Here we have shown evidence that finite 1D 3d metal chains can sustain both short- and long-range ferromagnetic order, and that parameters such as the size of the local magnetic moments and anisotropy are strongly dependent on the dimensionality of the Co chains. Future investigations could address the persistence and extent of short-range magnetic order in the chains as a function of their length and temperature. □

1. Schneider, C. M. & Kirschner, J. in *Handbook of Surface Science* (eds Horn, K. & Scheffler, M.) 511–668 (Elsevier, Amsterdam, 2000).
2. Himpsel, F. J., Ortega, J. E., Mankey, G. J. & Willis, R. F. Magnetic nanostructures. *Adv. Phys.* **47,** 511–597 (1998).
3. Stamm, C. *et al.* Two-dimensional magnetic particles. *Science* **282,** 449–451 (1998).
4. Weinert, M. & Freeman, A. J. Magnetism of linear chains. *J. Mag. Magn. Mater.* **38,** 23–33 (1983).
5. Dorantes-Dávila, J. & Pastor, G. M. Magnetic anisotropy of one-dimensional nanostructures of transition metals. *Phys. Rev. Lett.* **81,** 208–211 (1998).
6. Pratzer, M. *et al.* Atomic-scale magnetic domain walls in quasi-one-dimensional Fe nanostripes. *Phys. Rev. Lett.* **87,** 127201-1–127201-4 (2001).
7. Landau, L. D. & Lifshitz, E. M. *Statistical Physics* Vol. 5, 482 (Pergamon, London, 1959).
8. Ising, E. Beitrag zur Theorie des Ferromagnetismus. *Z. Phys.* **31,** 253–258 (1925).
9. Mermin, N. D. & Wagner, H. Absence of ferromagnetism in one- or two-dimensional isotropic Heisenberg models. *Phys. Rev. Lett.* **17,** 1133–1136 (1966).
10. Lieb, E. H. & Mattis, D. C. *Mathematical Physics in One Dimension* (Academic, New York, 1966).
11. De Jongh, L. J. & Miedema, A. R. Experiments on simple magnetic model systems. *Adv. Phys.* **23,** 1–260 (1974).
12. Röder, H. *et al.* Building one- and two-dimensional nanostructures by diffusion-controlled aggregation at surfaces. *Nature* **366,** 141–143 (1993).
13. Gambardella, P. *et al.* One-dimensional metal chains on Pt vicinal surfaces. *Phys. Rev. B* **61,** 2254–2262 (2000).
14. Elmers, H. J. *et al.* Submonolayer magnetism of Fe(110) on W(110): finite width scaling of stripes and percolation between islands. *Phys. Rev. Lett.* **73,** 898–901 (1994).
15. Hauschild, J., Elmers, H. J. & Gradmann, U. Dipolar superferromagnetism in monolayer nanostripes of Fe(110) nanostripes on vicinal W(110) surfaces. *Phys. Rev. B* **57,** R677–R680 (1998).
16. Shen, J. *et al.* Magnetism in one dimension: Fe on Cu(111). *Phys. Rev. B* **56,** 2340–2343 (1997).
17. Gambardella, P. *et al.* Co growth on Pt(997): from monatomic chains to monolayer completion. *Surf. Sci.* **449,** 93–103 (2000).
18. Stöhr, J. & Nakajima, R. Magnetic properties of transition-metal multilayers studied with XMCD spectroscopy. *IBM J. Res. Develop.* **48,** 73–88 (1998).
19. Wu, R., Li, C. & Freeman, A. J. Structural, electronic and magnetic properties of Co/Pd(111) and Co/Pt(111). *J. Mag. Magn. Mater.* **99,** 71–80 (1991).
20. Thole, B. T., Cara, P., Sette, F. & van der Laan, G. X-ray circular dichroism as a probe of orbital magnetization. *Phys. Rev. Lett.* **68,** 1943–1946 (1992).
21. Weller, D. *et al.* Microscopic origin of magnetic anisotropy in Au/Co/Au probed with x-ray magnetic circular dichroism. *Phys. Rev. Lett.* **75,** 3752–3755 (1995).
22. Chen, C. T. *et al.* Experimental confirmation of the XMCD sum rules for iron and cobalt. *Phys. Rev. Lett.* **75,** 152–155 (1995).
23. Tischer, M. *et al.* Enhancement of orbital magnetism at surfaces: Co on Cu(100). *Phys. Rev. Lett.* **75,** 1602–1605 (1995).
24. Dürr, H. A. *et al.* Spin and orbital magnetization in self-assembled Co clusters on Au(111). *Phys. Rev. B* **59,** R701–R704 (1999).
25. Crangle, J. & Scott, W. R. Dilute ferromagnetic alloys. *J. Appl. Phys.* **36,** 921–928 (1965).
26. Bate, G. Magnetic recording materials since 1975. *J. Magn. Magn. Mater.* **100,** 413–424 (1991).
27. Fróta-Pessoa, S., Muniz, R. B. & Kudrnovský, J. Exchange coupling in transition-metal ferromagnets. *Phys. Rev. B* **62,** 5293–5296 (2000).
28. Wernsdorfer, W. *et al.* Experimental evidence of the Néel-Brown model of magnetization reversal. *Phys. Rev. Lett.* **78,** 1791–1794 (1997).

....

An ordered mesoporous organosilica hybrid material with a crystal-like wall structure

Shinji Inagaki*, **Shiyou Guan***†, **Tetsu Ohsuna**‡ & **Osamu Terasaki**§

* *Toyota Central R&D Laboratories, Inc., Nagakute, Aichi, 480-1192, Japan*
‡ *Institute for Materials Research, Tohoku University, Sendai 980-8577, Japan*
§ *Department of Physics and CREST, JST, Graduate School of Science, Tohoku University, Sendai 980-8578, Japan*
† *Present address: Sanyo Chemical Industry, Ltd, Higashiyama, Kyoto, 605-0995, Japan*

....

Surfactant-mediated synthesis strategies are widely used to fabricate ordered mesoporous solids[1–6] in the form of metal oxides[7], metals[8], carbon[9] and hybrid organosilicas[10–14]. These materials have amorphous pore walls, which could limit their practical utility. In the case of mesoporous metal oxides, efforts to crystallize the framework structure by thermal[15,16] and hydrothermal treatments[17] have resulted in crystallization of only a fraction of the pore walls. Here we report the surfactant-mediated synthesis
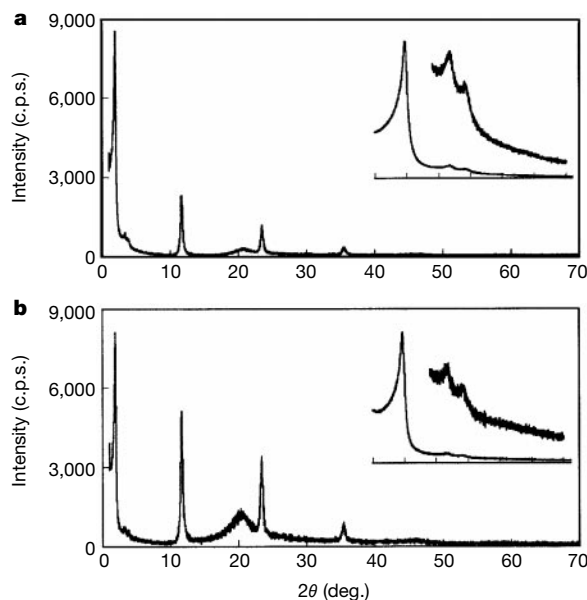

Figure 1 Powder X-ray diffraction patterns of mesoporous benzene–silicas. **a**, Material after removal of surfactants. **b**, As-made material containing surfactants. Patterns in the low-angle region ($1 < 2\theta < 7$) are shown magnified in the insets. These materials have both mesoscale ($d = 45.5$, 26.0 and 22.9 Å) and molecular-scale ($d = 7.6$, 3.8 and 2.5 Å) periodic structures.

of an ordered benzene–silica hybrid material; this material has an hexagonal array of mesopores with a lattice constant of 52.5 Å, and crystal-like pore walls that exhibit structural periodicity with a spacing of 7.6 Å along the channel direction. The periodic pore
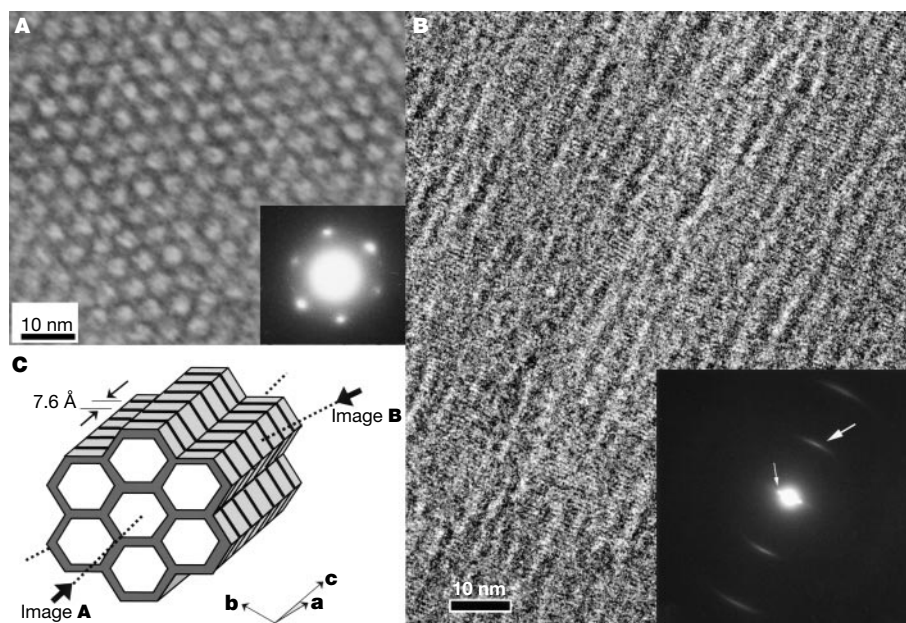

Figure 2 TEM images, electron diffraction patterns and the resulting structural model of mesoporous benzene–silica. The images and the patterns are arranged in the correct orientation relation—that is, the diffraction spots and corresponding lattice planes are normal to each other. **A,** Image and pattern taken with [001] incidence, parallel to the channels. Uniform mesopores with a diameter of 38 Å are arranged in a hexagonal manner. **B,** Image and pattern taken with [100] incidence, perpendicular to the channels. Many lattice fringes with a spacing of 7.6 Å are observed in the pore walls. The wavy contrast, which is perpendicular to the lattice fringes, with a spacing of 45.5 Å ($d = \sqrt{3}a/2$) are also discernible. Note that we cannot observe the contrast of 7.6-Å and 45.5-Å spacings at the best condition simultaneously for both, because the dependence of the contrast transfer function of the objective lens on focus condition is different for both. The electron diffraction pattern also shows diffused spots due to the 7.6-Å periodicity (large arrow) in the perpendicular direction to the spots due to channel arrangement with $d = 45.5$ Å (small arrow). **C**, Schematic model of mesoporous benzene–silica derived from the results of the TEM images and electron diffraction patterns.